Optically triggered infrared photodetector

Íñigo Ramiro[ξ*], *Antonio Martí*[ξ], *Elisa Antolín*[ξ], *Esther López*[ξ], *Alejandro Datas*[ξ], *Antonio Luque*[ξ], *José M. Ripalda*[ψ] *and Yolanda González*[ψ].

[ξ]Instituto de Energía Solar, ETSI Telecomunicación, Universidad Politécnica de Madrid, 28040 Madrid, Spain.

[ψ]Instituto de microelectrónica de Madrid, CNM (CSIC), C/Isaac Newton 8, PTM, 28760 Tres Cantos, Madrid, Spain.

KEYWORDS

Photodetector, infrared, quantum dots, intermediate band.

ABSTRACT

We demonstrate a new class of semiconductor device: the Optically Triggered Infrared Photodetector (OTIP). This photodetector is based on a new physical principle that allows the detection of infrared light to be switched ON and OFF by means of an external light. Our experimental device, fabricated using InAs/AlGaAs quantum-dot technology, demonstrates normal incidence infrared detection in the 2–6 μm range. The detection is optically triggered by a 590-nm light-emitting diode. Furthermore, the detection gain is achieved in our device without an increase of the noise level. The novel characteristics of OTIPs open up new possibilities for third generation infrared imaging systems[1].

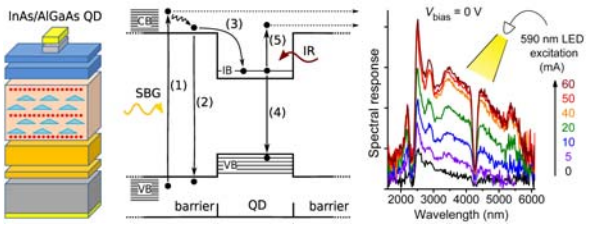

Infrared (IR) photodetectors are used in a wide variety of applications in the scientific, medical, industrial and military areas. In the mid (3–5 μm) and long (8–12 μm) wavelength infrared (MWIR and LWIR) atmospheric windows, there are currently two main competing IR photodetector technologies: variable, low-bandgap photodiodes and photoconductive devices that exploit the quantum confinement in wide-gap materials, such as quantum well IR photodetectors (QWIP)[2, 3] and quantum dot IR photodetectors (QDIP)[4]. Photodiodes extract photo-excited carriers from a p–n junction under reverse bias. Photoconductors allow light detection due to the change in the device conductivity caused by the increase in the number of free carriers when light is absorbed. Photoconductors require voltage biasing to operate too.

HgCdTe[5, 6] photodiodes have been the leading performing technology for the last half century, but they present some disadvantages: substrates for HgCdTe growth are scarce and expensive, and large-area growth inhomogeneity hinders the fabrication of large-format photodetectors[7]. For this reason different low bandgap materials, such as InAsSb supperlattices[8, 9] or, more recently, InAsBi[10] have been investigated as promising alternatives for the MWIR range. QWIPs, and specially QDIPs, have been regarded as possible alternatives in the MWIR and LWIR ranges, for they are technologically mature and their detection wavelength can be engineered over these ranges, up to 12 μm[11-13]. However, they cannot, so far, compete in performance with their photodiode counterpart.[4] With that goal, big efforts are being made for achieving increased responsivities and lower dark currents[14-16]. The difficulty of this task lies in the dependency of

both parameters with the applied voltage in voltage-driven photodetectors. In this respect, good performance results have been obtained in photodiodes working in photovoltaic mode[17].

In this letter, we present and characterize, for the first time, a new type of IR photodetector that we call "Optically Triggered Infrared Photodetector" (OTIP). Along this work we will describe the novel physical principle responsible for IR light detection in the OTIP. We will demonstrate a successful implementation of the OTIP using InAs/AlGaAs quantum dots (QDs) technology. We will experimentally show that, in contrast with the aforementioned established technologies and others[18], the OTIP has the following differentiating features: 1) it is optically triggered, hence it can be commuted with light in optical communication systems, 2) it does not require an electrical power supply, and 3) the external light-bias provides photo-detection gain without increasing the detector noise level. In addition to these features, our device shares, in principle, the intrinsic advantages of photo-detection using semiconductor QDs: control of peak response wavelength, the possibility of multiband detection[19], and the use of a mature and available technology.

Figure 1 shows the simplified device structure of the OTIP, its band diagram and an equivalent circuit. It consists of a QD-region sandwiched between conventional p– and n–semiconductors. In the QD-stack region, the electron confinement in the QDs allows the classification of the electron energy levels into three simplified groups (Figure 1b): the conduction band (CB), formed by the electron states with energy above the conduction band edge of the barrier material; the valence band (VB), consisting of the electron states with energies lower than the valence band edge of the barrier, plus the highly packed confined electron states in the valence band potential well of the QD; and the intermediate states, formed by the confined electron states in the conduction band potential well of the QD. We call these intermediate states the "intermediate

band" (IB) because the operation of the OTIP will be mostly described based on the intermediate band solar cell (IBSC) theory framework.[20, 21]

The detection of IR light in our device works as follows: IR photons, in the mid-long wavelength range, promote electronic transitions from the IB to the CB. These transitions are represented by arrow "5" in Figure 1b and by the current generator J_{IR} in the circuit model in Figure 1c. However, in an ideal device, the absorption of these IR photons would not yet produce any photocurrent because there is no path for the electrons pumped to the CB to return to the IB and repopulate it. Hence, once electrons have circulated through the external circuit, returning to the IB would require some mechanism capable of pumping these electrons back from the VB to the IB. This pumping mechanism does not exist when the device is illuminated only with mid-long wavelength IR radiation. When explained in terms of the circuit model in Figure 1c, returning to the IB would imply an electrical current flowing in reverse through diode D2. Because we assume D2 to be ideal, this current flow is not possible. Therefore, when illuminated with IR radiation only, the electrons that have been pumped to the CB recombine back to the IB through diode D1 and no external photocurrent is detected.

We will now see how this operation mode changes if, prior to the detection of IR light, the device is illuminated with a supra-bandgap biasing light source (SBG in Figure 1b) whose photons, when absorbed, are capable of pumping electrons from the VB to the CB (arrow "1" in Figure 1b). In the absence of the IR light, some of the electrons generated by the SBG will circulate through the external circuit. Not all the generated electrons will circulate because, in general, some will recombine directly from the CB to the VB (arrow "2" in Figure 1b) and some will also recombine to the VB but via the IB (arrows "3" and "4" in Figure 1b). In the circuit model in Fig. 1c, the photo-excitation of electrons by the SBG is represented by the current

generator J_G, and the recombination paths to the VB that we have described are represented by current J_{D3} (through diode D3) when not going via the IB, and by currents J_{D1} and J_{D2} (through diodes D1 and D2, respectively) when assisted by the IB. Therefore, the current through the external circuit when there is no IR light, J_{SC0}, is given by $J_{SC0} = J_G - J_{D3} - J_{D1}$. However, when IR illumination is added, the net carrier recombination from the CB to the IB diminishes. As a consequence, the current though the external circuit is modified by $\Delta J_{SC,}$ which verifies that $J_{SC} = J_G - J_{D3} - (J_{D1} - J_{IR}) = J_{SC0} + \Delta J_{SC}$, where $\Delta J_{SC} = J_{IR}$.

Figure 2 illustrates the detailed semiconductor layer structure with which we have implemented our OTIP. The material growth was carried out by molecular beam epitaxy. The OTIP device structure is grown on a (100) n-GaAs substrate. Ten layers of InAs QDs are grown embedded in 60-nm n–doped $Al_{0.35}Ga_{0.65}As$ barriers. The barriers are doped with approximately 10 Si atoms per QD in order to highly populate the IB with electrons and increase the IR absorption[22]. However, doping of the barriers is not strictly necessary for the OTIP operation since, even in the undoped case, part of the QDs (those which are closest to the n–emitter) are filled with electrons because they are placed in a space charge region[23].

The InAs deposited for the QDs formation is two monolayers thick. The barriers separating the QDs from the p and n–regions are 130 nm thick. The QD-stack is sandwiched between a 200-nm p–doped and a 500-nm n–doped $Al_{0.35}Ga_{0.65}As$ emitter. Above and below the emitters, a 50-nm $Al_{0.78}Ga_{0.22}As$ window layer and a 105-nm $Al_{0.41}Ga_{0.59}As$ back surface field layer, respectively, are grown with the aim of minimizing the recombination of photo-generated carriers in the surfaces of the device. Metal contacts are placed on the top and at the bottom of the structure. Finally, a 30-nm highly doped p-GaAs contact layer is grown above the window layer to allow the formation of ohmic contacts.

Standard photolithography techniques were used for processing the sample. The back contact was made by evaporating 100 nm of Au-Ge alloy, 25 nm of Ni, and 300 nm of Au, and followed by rapid thermal annealing (370 ºC, 180 s). The front contact was made by evaporating 45 nm of Cr and 330 nm of Au. After lift-off, wet etching removed the p-GaAs contact layer, which remained only underneath the front metal grid. MESA etching completed the processing, delimiting 1 mm-radius circular devices. Samples were mounted on a copper disk that acted as the contact and a heat sink.

Figure 3a shows the experimental spectral response (ΔJ_{SC} divided by the incident SBG power, P_{SBG}) of our device measured at a temperature (T) of 9 K as a function of the wavelength of the normal incident IR photons. In the experiment, which will be described in detail later on, these photons come from an IR emitter after passing through a monochromator and adequate optical filters. The sample was simultaneously illuminated by a 590-nm (2.1 eV) light-emitting diode (LED) – note that, at T = 9 K, the bandgap of our device is 2.0 eV, which is smaller than the LED photon emission energy. Several LED-biasing currents (LBC) were used in the experiment, ranging from 0 to 60 mA, as indicated in the legend. This LED plays the role of the SBG as explained above.

The results in Figure 3a demonstrate that the OTIP operates as an optically triggered IR photodetector since, first, it responds to the MWIR light and, in addition, this response increases with the irradiance of the LED (which is modulated by the LBC), being nearly zero when the LED is OFF. The reason why the photocurrent induced in the OTIP is not exactly zero when the LED is OFF, as expected by the theory for the ideal device explained above, will be discussed later. Proper OTIP operation was demonstrated also at T = 60 K. This result is presented in the Supporting information. At higher temperatures the measured signal was reduced and finally met

the noise level of the measurement (at around 100 K). A possible explanation for this reduction in the response is that thermal excitation of electrons from the IB to the CB competes with optical excitation, thus reducing the sensitivity of the device.

We used the experimental set-up depicted in Figure 3b for the measurements. This set-up is a modification of the one described in ref.[24], which served to initially demonstrate the photocurrent due to MWIR illumination in QD-based IBSCs. Commercially available 590-nm LEDs and a Newport 140 W IR SiC lamp were used as the SBG and the IR light sources, respectively. The IR source was chopped and directed into a three-grating Newport 1/4 m monochromator. A set of IR long-pass optical filters was placed at the exit of the monochromator to minimize the impact of residual broadband and second order light on the measurements. Light was directed to be normally incident onto the sample. The sample was placed in a closed-cycle He-cryostat and connected to a low-noise Stanford Research Systems SR570 transimpedance amplifier. This amplifier also served as the voltage source to bias the sample. The final signal detection was made using a Stanford Research Systems SR830 lock-in amplifier to measure at the chopping frequency (177 Hz). All the results presented in Figure 3 were measured for zero voltage bias.

The results presented in Figure 3a demonstrate IR detection in the 2000–6000 nm range, peaking at 3350 nm. This broadband energy spectrum (≈ 400 meV) is explained by the combination of possible electronic transitions between the bound states in the conduction band of the QDs and/or between these bound states and the extended states in the CB.[25] The measured detection range arises as a result of a large energy difference between the IB and the CB due to the large difference in the bandgaps of the InAs and the $Al_{0.35}Ga_{0.65}As$. The detection range can be tuned to longer wavelengths by changing the QD material and/or the host material or by modifying the growth conditions of the QDs. The response valley at approximately 2340 nm is

an artifact in the measurement that was caused by the optical filters. The detection valley measured at approximately 4260 nm corresponds to the atmospheric absorption of CO_2.

It was previously stated that, in an ideal device, no photocurrent would be produced under only IR illumination. However, our practical OTIP can still marginally detect IR light when the LED is switched OFF. This behavior is explained by diode D2 not being ideal and thus capable, due to reverse leakage, of providing a path for returning to the IB to the electrons in the VB. In this situation, the measured ΔJ_{SC} corresponds to the reverse current flowing through D2 and is limited by its reverse saturation current.

To further characterize the OTIP gain, Figure 3c shows the integrated value of the photocurrents presented in Figure 3a (normalized to the value obtained for 0 mA LBC) as a function of the measured LED irradiance (normalized to the value for 60 mA LBC). The irradiance of the LED was measured using a Newport calibrated Si-photodiode. It can be seen that the optically triggered detection increases with the LED irradiance, but at a decreasing rate. This suggests that the photo-detection might saturate at a sufficiently high SBG bias illumination. This hypothesis is further supported by voltage dependent photocurrent measurements presented in the Supporting Information. The maximum measured gain factor is 6.2. The noise level remained unchanged for all the values of the bias current. This is shown in Figure 3d, where a magnification of the 1000–2000 nm measured range is shown for 0 and 60 mA LBCs. However, it would be expected that an increase in the light biasing, which implies a larger J_{SC0}, would also increase the measurement noise. The fact that the noise level remained unchanged implies that the light biasing was not the dominant noise source in our measurements. As a consequence, the gain in photo-detection can be understood as a gain in the signal-to-noise ratio and, hence, in the detectivity. The measured responsivity of our device (in the order of 0.1

mA/W) is lower than that of state-of-the-art voltage-driven IR photodetectors (up to hundreds of mA/W). Further studies are needed to increase the performance of this new kind of devices. Nonetheless, the optical commutation of the OTIP opens up possibilities for new detection application. For this reason, it is important to experimentally evaluate what photon energies are able to activate the IR detection of the OTIP.

The set-up presented in Figure 3b was modified to measure the two-photon photocurrent as described in ref.[24]. In this case, a monochromator diffracting the light from a halogen lamp provided a continuous-wave primary light source. The light from an IR light source, filtered with a 350-μm-thick GaSb wafer (so that only photons with energy lower than the GaSb gap, 0.73 eV, could reach the sample) was chopped and used as a secondary source. Visible and near-IR wavelengths were swept with the primary source to evaluate what photon energies, in combination with the broadband IR illumination, led to the production of photocurrent in the OTIP. Figure 4 shows the photocurrent response (open circles) of the studied device as a function of the incident wavelength of a monochromatic beam in combination with normal broadband IR illumination. The measurement was performed at T = 9 K. For energies above the $Al_{0.35}Ga_{0.65}As$ bandgap, E_G, there is a wavelength-dependent response. This means that the extracted photocurrent is indeed produced by the combination of high and low energy photons illuminating the sample. The photocurrent drops abruptly at E_G and then, for longer wavelengths, it decays slowly. For wavelengths longer than 1300 nm, the measured photocurrent becomes constant. We have called this constant value of the photocurrent the “offset-level”. This value can be understood as the photocurrent produced as a result of the broadband IR illumination only, which promotes electrons from the IB to the CB. As described in the main text, if the diode D2 between the VB and the IB is not ideal, its reverse current can close the loop for electrons in

the VB to return to the IB. The result of subtracting the offset level from the measurement is also plotted (solid line). This curve more clearly illustrates the photocurrent response of the OTIP due to the simultaneous illumination with two photons of different energy, one of them in the MWIR. The supra-bandgap response, in this curve, remains high, but the sub-bandgap response decreases quickly for longer wavelengths until it is no longer detectable beyond 1300 nm. This result corroborates that our device produces IR detection gain due to a secondary-light bias for a wide range of supra-bandgap energies. The emission energy of the LED used for the measurements presented in Figure 3 is indicated in Figure 4.

In conclusion, we have proposed and experimentally characterized a novel IR photodetector, showing response to normally-incident light in the 2–6 μm range. The inclusion of QDs in-between a p-n junction allows IR detection to be switched ON and OFF by means of external light biasing at short-circuit conditions. We have demonstrated that OTIP operation can be driven by a continuous range of photon energies above the bandgap of the device. We have measured a gain in photo-detection up to 6.2 using a 690 nm LED as external light source, with no increase in the measurements noise. Our device breaks with the traditional trade-off between responsivity and dark current, present in voltage-driven photodetectors. We believe that this new device opens up new possibilities for implementing third generation infrared imaging systems. The fact that it does not need electrical power supply and that it can be optically commuted, make the OTIP attractive for optical communications.

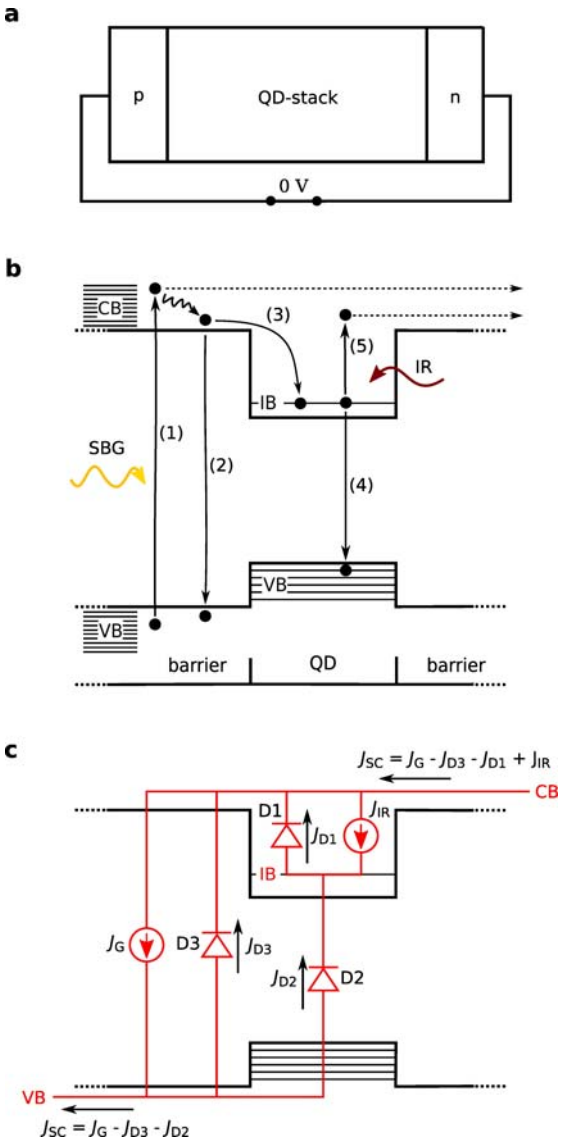

Figure 1. An illustration of the OTIP structure and operation. (a) The simplified semiconductor structure of the OTIP. (b) The 1D band diagram of a barrier/QD/barrier semiconductor zone. The electrons in the barriers are pumped from the VB to the CB due to the SBG light source (1). Subsequently, they either are extracted as photocurrent, relax to the VB (2) or relax to the IB in the QDs (3). Electrons in the QDs are pumped from the IB to the CB due to the IR illumination (5) or relaxed from the IB to the VB (4). (c) The equivalent circuit of the processes described in (a). J_G, and J_{IR} represent the pumping of electrons due to the SBG and IR light sources,

respectively. J_{D1}, J_{D2} and J_{D3} represent the CB→IB, the IB→VB and the CB→VB electron relaxations, through diodes D1, D2 and D3, respectively. J_{SC} is the short-circuit current flowing through the detector.

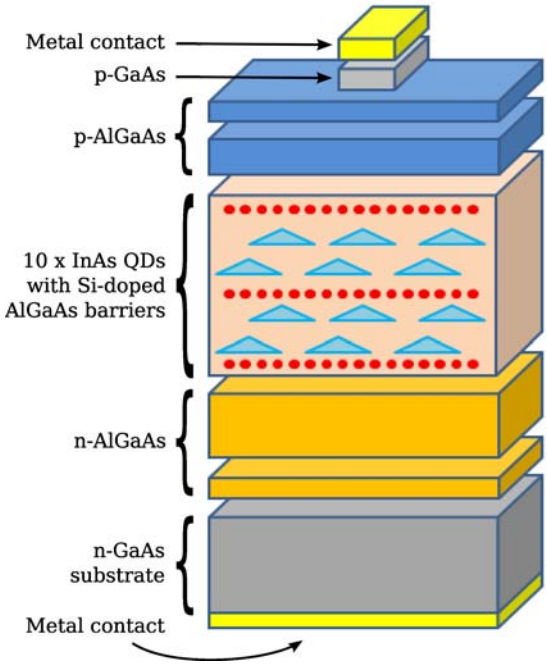

Figure 2. A detailed layer structure of the experimental device. Ten layers of InAs QDs are sandwiched between Si–doped $Al_{0.35}Ga_{0.65}As$ barriers. The QD-stack is placed between p and n–doped $Al_{0.35}Ga_{0.65}As$ emitters.

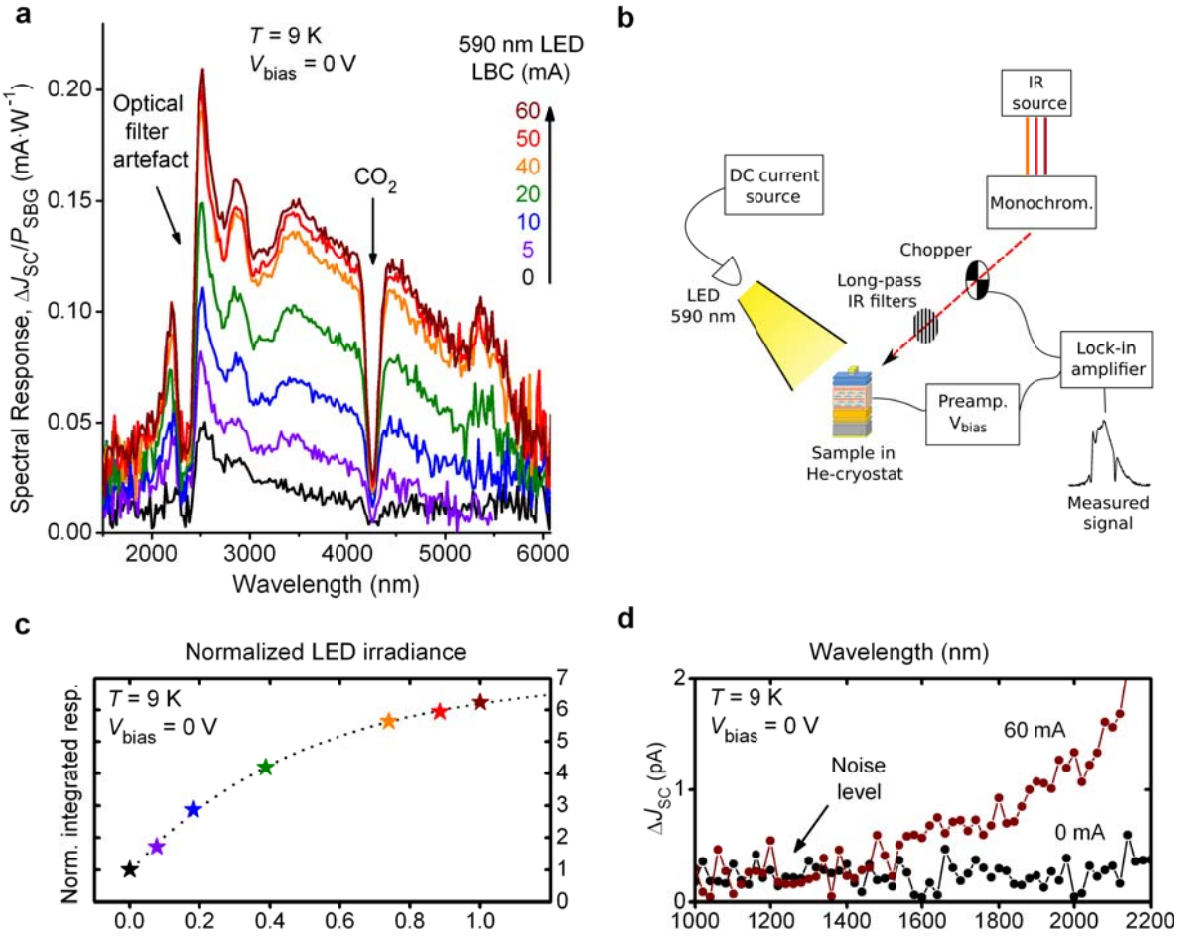

Figure 3. The dependence of the spectral response with the supra-bandgap LED light bias of the OTIP under short-circuit conditions. (a) The measured spectral response at T = 9 K for various values of the LBC. (b) A diagram of the set-up used for performing the photocurrent measurements. (c) The normalized integrated values of the photocurrents as a function of the normalized LED irradiance. The dotted line is a guide to the eye. (d) A magnification of the 1000–2000 nm range of the photocurrent measurements corresponding to Figure 3a for the 0 and 60 mA LBC cases. The noise level is indicated.

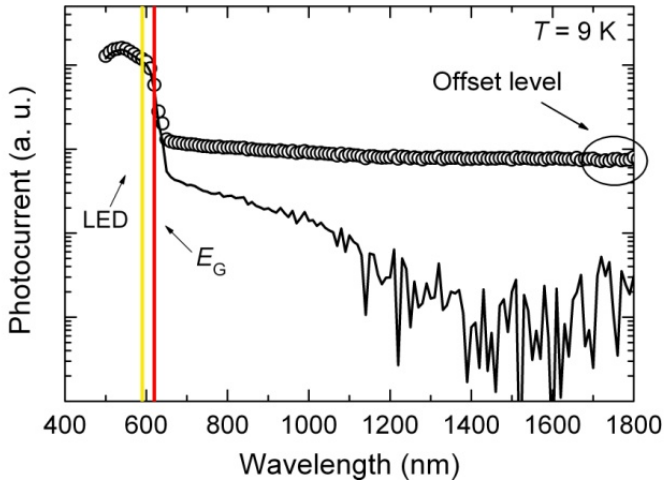

Figure 4.Semilog plot of the measured two-photon photocurrent as a function of the monochromatic beam wavelength (open circles), and the result of subtracting the wavelength-independent photocurrent response, or "offset level", from that measurement (solid line). The bandgap, E_G, of the $Al_{0.35}Ga_{0.65}As$ at T = 9 K and the energy of the LED used in this work are indicated.

ASSOCIATED CONTENT

Supporting information

The voltage bias dependency of the photo-response of the OTIP, and the demonstration of proper OTIP operation at T = 60 K. This material is available free of charge via the Internet at http://pubs.acs.org.

AUTHOR INFORMATION

Corresponding author:

*E-mail: inigo.ramiro@ies-def.upm.es

AUTHOR CONTRIBUTIONS

All authors collaborated in the elaboration of the manuscript. J. M. R. and Y. G. fabricated the semiconductor material. A. D. and I. R. did the device processing. E. A., A. M. and I. R. designed the experiments. I. R. performed the experiments. A. M. and A. L. coordinated the project.

ACKNOWLEDGMENT

The authors acknowledge the Spanish Government for funding through the National Research Program PROMESA (ENE2012-37804-C02).

REFERENCES

1. Rogalski, A.; Antoszewski, J.; Faraone, L. Journal of Applied Physics 2009, 105, (9), 091101.

2. Levine, B. F. Journal of Applied Physics 1993, 74, R1.

3. Manasreh, M. O., Semiconductor quantum wells and superlattices for long-wavelength infrared detectors. Artech House: 1993.

4. Martyniuk, P.; Rogalski, A. Progress in Quantum Electronics 2008, 32, (3), 89-120.

5. Rogalski, A. Reports on Progress in Physics 2005, 68, (10), 2267.

6. Tennant, W. E. Progress in Quantum Electronics 2012, 36, (2), 273-292.

7. Barve, A. V.; Lee, S. J.; Noh, S. K.; Krishna, S. Laser & Photonics Reviews 2010, 4, (6), 738-750.

8. Smith, D. L.; Mailhiot, C. Journal of Applied Physics 1987, 62, (6), 2545-2548.

9. Kurtz, S. R.; Dawson, L. R.; Zipperian, T. E.; Lee, S. R. Applied Physics Letters 1988, 52, (19), 1581-1583.

10. Sandall, I. C.; Bastiman, F.; White, B.; Richards, R.; Mendes, D.; David, J. P. R.; Tan, C. H. Applied Physics Letters 2014, 104, (17), 171109.

11. Kim, E.-T.; Chen, Z.; Madhukar, A. Applied Physics Letters 2001, 79, (20), 3341-3343.

12. Gunapala, S. D.; Bandara, S. V.; Hill, C. J.; Ting, D. Z.; Liu, J. K.; Rafol, S. B.; Blazejewski, E. R.; Mumolo, J. M.; Keo, S. A.; Krishna, S. Quantum Electronics, IEEE Journal of 2007, 43, (3), 230-237.

13. Aivaliotis, P.; Zibik, E. A.; Wilson, L. R.; Cockburn, J. W.; Hopkinson, M.; Airey, R. J. Applied Physics Letters 2007, 91, (14), 143502-143502-3.

14. Liu, H.; Zhang, J. Optics & Laser Technology 2012, 44, (5), 1536-1542.

15. Asano, T.; Madhukar, A.; Mahalingam, K.; Brown, G. J. Journal of Applied Physics 2008, 104, (11), 113115.

16. Wang, S. Y.; Lin, S. D.; Wu, H. W.; Lee, C. P. Applied Physics Letters 2001, 78, (8), 1023-1025.

17. Kim, J. D.; Kim, S.; Wu, D.; Wojkowski, J.; Xu, J.; Piotrowski, J.; Bigan, E.; Razeghi, M. Applied Physics Letters 1995, 67, (18), 2645-2647.

18. Rogalski, A. Infrared Physics & Technology 2002, 43, (3), 187-210.

19. Varley, E.; Lenz, M.; Lee, S. J.; Brown, J. S.; Ramirez, D. A.; Stintz, A.; Krishna, S.; Reisinger, A.; Sundaram, M. Applied Physics Letters 2007, 91, (8), 081120.

20. Luque, A.; Martí, A. Physical Review Letters 1997, 78, (26), 5014-5017.

21. Luque, A.; Martí, A.; Stanley, C. Nature Photonics 2012, 6, (3), 146-152.

22. Attaluri, R.; Annamalai, S.; Posani, K.; Stintz, A.; Krishna, S. Journal of Vacuum Science & Technology B: Microelectronics and Nanometer Structures 2006, 24, (3), 1553-1555.

23. Martí, A.; Antolín, E.; Cánovas, E.; López, N.; Linares, P. G.; Luque, A.; Stanley, C. R.; Farmer, C. D. Thin solid films 2008, 516, (20), 6716-6722.

24. Martí, A.; Antolín, E.; Stanley, C. R.; Farmer, C. D.; Lopez, N.; Díaz, P.; Canovas, E.; Linares, P. G.; Luque, A. Physical Review Letters 2006, 97, (24), 247701-4.

25. Luque, A.; Martí, A.; Mellor, A.; Fuertes Marrón, D.; Tobías, I.; Antolín, E. Progress in Photovoltaics: Research and Applications 2013, 21, 658-667.